

J-integral calculation by domain integral technique using adaptive finite element method

Sutthisak Phongthanapanich

*Mechanical Engineering Technology Department, College of Industrial Technology,
King Mongkut's University of Technology North Bangkok, Bangkok 10800, Thailand*

Kobsak Potjananapasiri and Pramote Dechaumphai[†]

*Mechanical Engineering Department, Faculty of Engineering, Chulalongkorn University,
Bangkok 10330, Thailand*

(Received November 30, 2005, Accepted December 28, 2007)

Abstract. An adaptive finite element method for analyzing two-dimensional and axisymmetric nonlinear elastic fracture mechanics problems with cracks is presented. The *J*-integral is used as a parameter to characterize the severity of stresses and deformation near crack tips. The domain integral technique, for which all relevant quantities are integrated over any arbitrary element areas around the crack tips, is utilized as the *J*-integral solution scheme with 9-node degenerated crack tip elements. The solution accuracy is further improved by incorporating an error estimation procedure onto a remeshing algorithm with a solution mapping scheme to resume the analysis at a particular load level after the adaptive remeshing technique has been applied. Several benchmark problems are analyzed to evaluate the efficiency of the combined domain integral technique and the adaptive finite element method.

Keywords: adaptive finite element method; domain integral technique; *J*-integral; solution mapping.

1. Introduction

The *J*-integral is widely used and accepted as a fracture mechanics parameter for determining the intensity of the crack tip fields in elastic solids. For two-dimensional analysis without body forces and temperature gradients, this parameter is originally formulated as a path-independent line integral in which remote contours can give exactly the same result as contours near the crack tip (Rice 1968). In general situation, the global path-independence is ceased and the integration must be performed on the vanishingly small contour shrunk onto the crack tip (Moran and Shih 1987). Because of this small contour and the extent of the HRR singularity fields at the crack tip then the line integral is not suitable to implement numerically (Anderson 2005). Therefore many alternative forms of expressions have been derived and proposed to circumvent the difficulties (Aoki *et al.* 1981, Atluri 1982). The finite element method became the preferred numerical tool for analyzing the fracture problems, because the analysis of explicit cracks in finite element method is easily

[†] Professor, Corresponding author, E-mail: fmepdc@eng.chula.ac.th

handled by introducing cracks in the mesh (Dechaumphai *et al.* 2003, Nishioka 1997, Nishioka *et al.* 2001, Nishioka and Stan 2003). In order to make the numerical solution more accurate and simple to be determined by the finite element method, the divergence theorem is applied to convert the original line integral into the domain integral form.

In this paper, the J -integral is calculated by the domain integral technique. The 6-node triangular element is employed in the analysis as the non-crack-tip element. A layer of singular degenerated elements is used to surround the crack tip as the crack tip elements. Each element is a 9-node Lagrange rectangular element in which one edge is collapsed onto the crack tip where three crack tip nodes can displace independently, while the mid-edge nodes and the interior node are placed at their usual mid-positions (Li *et al.* 1985). An adaptive remeshing technique with a solution mapping scheme is then implemented to enhance the solution accuracy at every load step. The efficiency of the combined adaptive finite element and domain integral technique is evaluated by analyzing several two-dimensional and axisymmetric problems.

2. J -integral & domain integral technique

Under the quasi-static analysis with crack lying on the x_1 axis, the two dimensional J -integral is defined by Shih *et al.* (1986)

$$J = \lim_{\Gamma \rightarrow 0} \int_{\Gamma} (W \delta_{1i} - \sigma_{ij} u_{j,1}) n_i dC \quad (1)$$

where Γ is a limiting contour starting from the bottom crack face and ending at the top surface as illustrated in Fig. 1, W is the strain energy density, σ_{ij} are the stress tensors, u_i are the displacement vectors, δ_{ij} is the Kronecker's delta, and n_i is the outward normal vector to the vanishing contour Γ .

In the absence of crack face tractions, Eq. (1) for the closed curve $C = C_1 - \Gamma + C^+ + C^-$ as shown in Fig. 1 can be written in the form

$$J = \int_C (\sigma_{ij} u_{j,1} - W \delta_{1i}) m_i q_1 dC \quad (2)$$

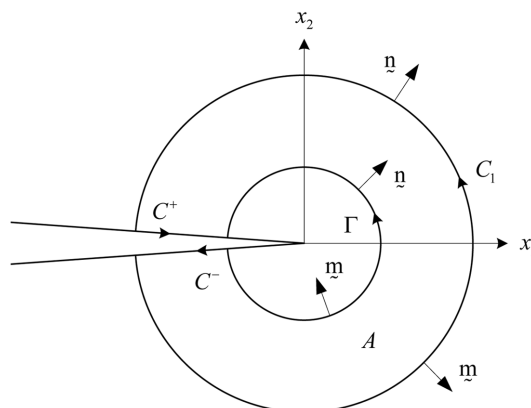


Fig. 1 Conventions on the J -integral expression and closed contour $C = C_1 - \Gamma + C^+ + C^-$ enclosing a simply connected region A

where q_1 is any sufficiently smooth function in the region enclosed by C provided that it is unity on Γ and zero on C_1 , and m_i is the outward normal vector to the domain surrounded by C . The divergence theorem is applied to Eq. (2) to yield the domain integral form

$$J = \int_A [(\sigma_{ij}u_{j,1} - W\delta_{1i})q_{1,i}]_i dA \tag{3}$$

where A is the area enclosed by C including the crack tip region because of $\Gamma \rightarrow 0$. With the presence of thermal strain, the total strain tensor ε_{ij} could be presented as the sum of the mechanical and the thermal strains

$$\varepsilon_{ij} = \varepsilon_{ij}^m + \beta T \delta_{ij} \tag{4}$$

where ε_{ij}^m represents the mechanical strain, β is the coefficient of thermal expansion and T is the temperature relative to the reference state. Under assumptions of the equilibrium equation without body forces and the strain energy density being the only function of mechanical strain, Eq. (3) can be expressed in the domain expression form

$$J = \int_A [(\sigma_{ij}u_{j,1} - W\delta_{1i})q_{1,i} + \beta \text{tr}(\sigma)T_{,1}q_1]_i dA \tag{5}$$

where $\text{tr}(\sigma)$ denotes the trace of σ_{ij} . Eq. (5) is domain-independent in the sense that any domain can be chosen for the purpose of calculating the J -integral. This characteristic of the domain integral technique is used to evaluate the accuracy of the computed J -integral by checking its equality of the results calculated from different integration domains.

For axisymmetric problems, the domain expression of the J -integral can be derived as a specialization of the three-dimensional formulation

$$J = \frac{1}{R} \int_A [(\sigma_{\omega\gamma}u_{\gamma,r} - W\delta_{r\omega})q_{r,\omega} + \beta \text{tr}(\sigma)T_{,r}q_r] r dA + \frac{1}{R} \int_A \left(\sigma_{\phi\phi} \frac{u_r}{r} - W \right) q_r dA \tag{6}$$

where r is the radius from the axis of symmetry to a point in the cross section, the indices ω and γ range over the cylindrical coordinates r and z , respectively. The q_r is a smooth function as in the two-dimensional expression, and $\sigma_{\phi\phi}$ and u_r/r are the hoop stress and strain, respectively. The $(\)_{,r}$ represents the partial derivative with respect to r , and R is the radius from the axis of symmetry to the crack tip.

3. Adaptive remeshing technique

The mesh generation implemented in this paper follows the Delaunay triangulation and the automatic point creation procedure which step-by-step explanation of these algorithms was presented in detail by Dechaumphai *et al.* (2003). The adaptive remeshing technique generates an entirely new mesh based on the solution obtained from a previous mesh. The second derivatives of any key variable such as von Mises stresses is used to determine the proper element sizes; that is, small elements are placed in the region where changes in the variable gradients are large especially

around crack tip. Practical experience found that this type of error indicator for the fracture mechanics problems, where regions such as crack tip has different strength, may cause inaccurate solution due to the inadequate refinement because the point spacing is scaled according to the maximum value of the second derivatives. This problem also found in the transient high-speed compressible flow problems which the adaptive remeshing algorithm previously proposed by Dechaumphai *et al.* (2003) provided deteriorate solutions.

To achieve higher solution accuracy, element sizes of two most inner layers around crack tip should not vary too rapidly. In order to overcome this problem, an element size scaling function, which scales the point spacing of point p_i within the range of χ_{\min} and χ_{\max} , has been used

$$\chi_i = \text{ScaleRange}\left(\frac{h_{\max} - dp_i}{h_{\max} - h_{\min}}, 0, 1, \chi_{\min}, \chi_{\max}\right) \quad (7)$$

The coefficient χ_i controls the point insertion in the regions of high solution gradient and eliminates excessive distortion of the regularity of the triangulation. The value of χ_{\min} limits the number of points insertion in the high gradient region, while the value of upper limit χ_{\max} allows to insert more points into the region with smaller solution gradient. When the adapted elements generated by this function are distorted in shape, the Alpha and Beta coefficients are incorporated to control the point density and the regularity of triangulation.

The adaptive mesh regeneration above has been developed and implemented as the Algorithm III presented by Dechaumphai *et al.* (2003) to provide better element shapes. The new mesh is constructed using the information from the previous or background mesh. Such mesh composes of small elements in the regions with large changes of the solution gradients, and large elements in the remaining regions where the changes of the solution gradients are small. Detailed process of adaptive remeshing technique is described as follows.

Algorithm AdaptiveRemeshing ($P, T, P0, \alpha, \beta, h_{\min}, h_{\max}, \chi_{\min}, \chi_{\max}, \text{threshold}$)

1. Let $P0, k = 1, \dots, n$ be the set of points of the background mesh.
2. Let P be the set of points and T be the set of triangles.
3. Read next interior point p_i of the background mesh from $P0$.
4. If $h_i > h_{\max}$ then go to step 3.
5. Search triangle t_i in T which contains the point p_i . Then calculate the centroid of the triangle t_i and define it as point p_q , and compute the point distribution function of point p_q by Eq. (8).

$$dp_q = \frac{1}{M} \sum_{j=1}^M |p_j - p_q| \quad (8)$$

where M is number of surrounding nodes to node q .

6. Compute the distance $d_m, m = 1, 2, 3$ from point p_q to all vertices of the triangle t_i .
7. Compute the χ_i coefficient, χ_i , for point p_i by using Eq. (7), and the average distance, $s_i = (d_1 + d_2 + d_3)/3$.
8. Perform the Xi-Alpha test for point p_q . If $(\chi_i * \alpha * h_i) \geq s_i$, then reject the point p_q and return to step 3.
9. Perform the Xi-Beta test for point p_q . If two out of three of $d_m < (\chi_i * h_{\min}/\beta)$ for any $m = 1, 2, 3$, then reject the point p_q and return to step 3.

10. Accept the point p_q for insertion by the Delaunay triangulation algorithm and add point p_q into P .
11. Repeat steps 3 to 10 until all points in P are considered.
12. Perform the Delaunay triangulation of the inserted points in P .
13. If number of accepted points greater than *threshold*, then go to step 3; otherwise stop the algorithm.

Since the proposed algorithm above does not guarantee the good mesh topology, the mesh relaxation (Frey 1991) based on an edge-swapping technique is included for well-shaped mesh improvement. The objective of this method is to make the topology of elements closer to equilateral triangles by swapping edges to equalize the vertex degrees (number of edges linked to each point) toward the value of six. Finally, the Laplacian smoothing is applied to smooth the meshes. The proposed algorithm is smart and robust enough for applying to hyperbolic, parabolic and elliptic problems (Phongthanapanich and Dechaumphai 2004, Phongthanapanich *et al.* 2006).

To evaluate the performance of the adaptive remeshing technique with the Delaunay triangulation, the specification of element size, h_i , is given as an analytic function defined for two-dimensional domain. The adaptive mesh generation process starts from an initial mesh generated in the domain, then the values of the element sizes at all points are computed by the given function. The mesh generation coupled with the adaptive remeshing procedure is iterated until the resulting mesh becomes globally stable. The iteration process is terminated if the total node increment is fewer than the specified number. The two examples of adaptive mesh generation with the analytical function for specifying element sizes presented herein are: (1) adaptive meshes along the centerline of a rectangular domain, and (2) an alpha-shape adaptive meshes in a square domain.

Adaptive Meshes along Centerline of a Rectangular Domain: The first example presents an adaptive mesh generation in a 3.0×5.0 rectangular domain. The element sizes at points in the domain are given by the distribution function

$$h(y) = 0.42 - \frac{1}{\sqrt{2\pi}\sigma} e^{-\left[\frac{y-\mu}{2\sigma}\right]^2} \tag{9}$$

where y is the variable and the values of μ and σ are constants equal to zero and one, respectively. Fig. 2 shows the series of adaptive meshes generated by three iterations based on a coarse initial mesh. The value of mesh generation coefficients, α , β , χ_{\min} , χ_{\max} are 0.5, 0.6, 0.75, and 1.10, respectively. Due to the prescribed distribution function in Eq. (9), small element sizes are specified around the centerline of the domain. The figure shows that size similarity of the adaptive meshes is generated along the narrow band around the centerline of the domain. The value of χ_{\min} limits the number of point insertion along the centerline of the domain, while the value of χ_{\max} allows more nodes to be inserted into the other regions.

The specification of scale range and χ_{\min} , χ_{\max} have strong effects on the resulting meshes as shown in Fig. 2. Without the scale range, the mesh is composed of small elements concentrated around line a (see Fig. 3) with progressively larger elements outwards as $h_a < h_b, h_c$. Hence, a mesh consisting of relatively uniform elements in a wider centerline band of the domain may be generated. This mesh has better physical correlation with the behaviors of shocks. The scale range function sorts the nodal spacing values into prescribed intervals according to χ_{\min} and χ_{\max} . In each interval, the generated element sizes are relatively uniform.

An Alpha-Shape Adaptive Meshes in a Square Domain: The third example presents an alpha-

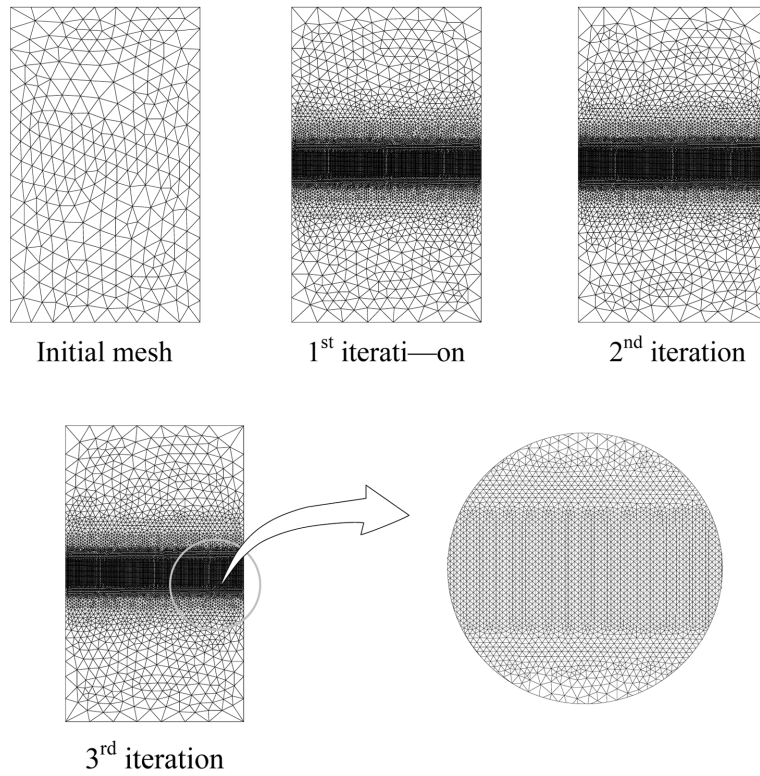


Fig. 2 Adaptive meshes along centerline of a rectangular domain

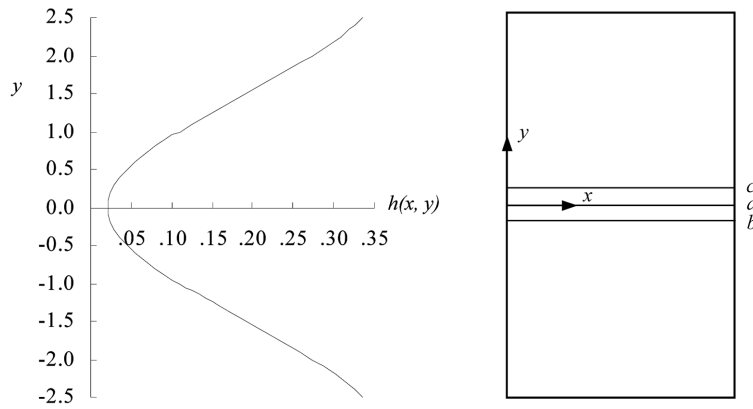


Fig. 3 Distribution of element sizes along the y direction

shape adaptive mesh generation in a square domain. The alpha shape function (Borouchaki *et al.* 1997) is used to calculate element sizes in an 8×8 square domain

$$h(x, y) = \begin{cases} \min(0.2(\lambda - 1)^3 + 0.005, 1.0) & \text{if } \lambda \geq 1 \\ \min(0.2(\lambda - 1)^2 + 0.01, 1.0) & \text{if } \lambda < 1 \end{cases} \quad (10)$$

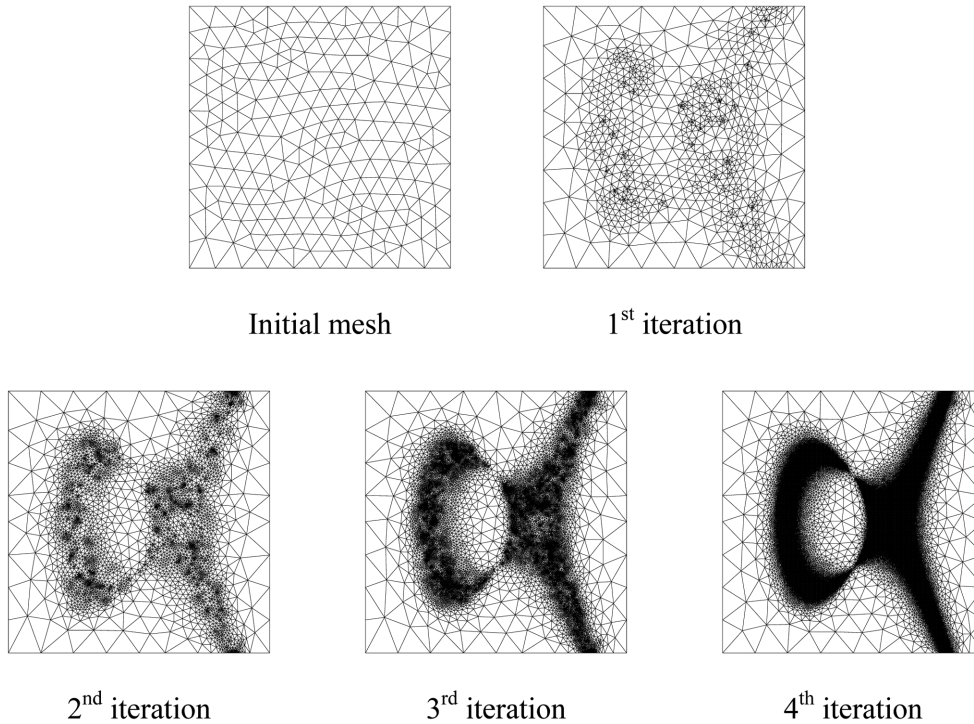


Fig. 4 An alpha-shape adaptive meshes in a square domain

where the value of parameter λ is determined from $x^3 - y^2 + 2 - 3\lambda x = 0$. Fig. 4 shows the sequence of four adaptive meshes generated from a coarse initial mesh. The value of mesh generation coefficients, α , β , χ_{\min} , χ_{\max} are 0.5, 0.6, 0.5, and 0.85, respectively. The smaller elements are generated along the alpha-shape in the domain while larger elements are generated in the other regions.

For practical problems, the preferred values of α and β are 0.5 and 0.6, respectively. In general, the acceptable ranges of these α and β values are 0.3~0.8, and 0.7~1.3, respectively. In addition, the values of 0.4 and 0.75 are chosen for χ_{\min} and χ_{\max} , respectively, for all test cases presented later in this paper.

4. Mapping of solution fields

In order to continue the analysis without restarting from the initial load level after a new mesh has been generated, the mapping of the displacement fields in the previous mesh onto the new adaptive mesh is needed. The 6-node triangular elements and the 9-node collapsed elements are used to form up the mesh. A layer of rosette singular degenerated elements which were originally the 9-node rectangular elements, with one edge on each element collapsed onto the crack tip location, is used to form up crack tip elements. This singular element improves the accuracy of the computed *J*-integral because its displacement gradients contain terms of order $(1/r)$, which is consistent with the continuum crack tip fields for elastic-perfectly plastic bodies (Li *et al.* 1985). In this paper, two

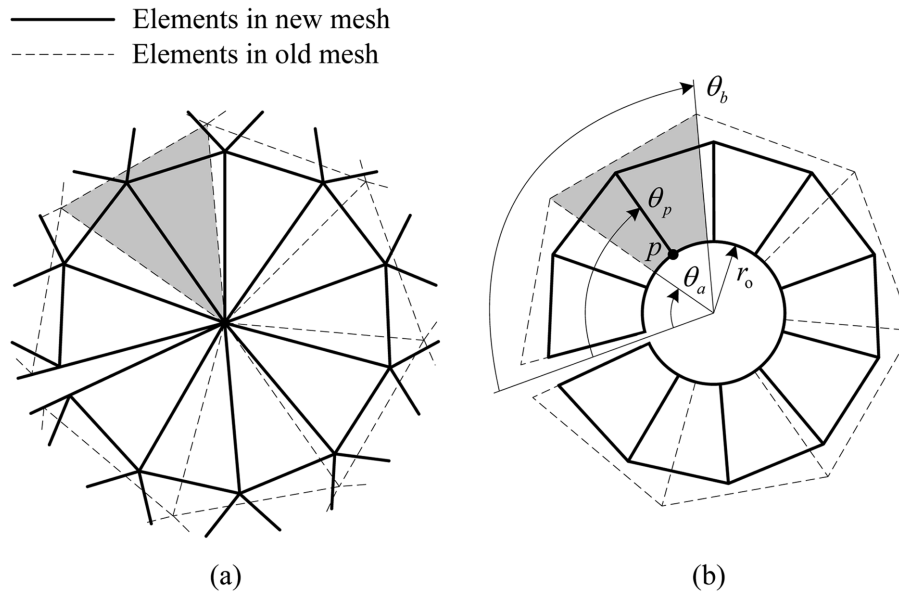


Fig. 5 (a) Crack tip elements in the new and old meshes and (b) crack tip elements as crack tip nodes placed a distance r_o from the crack tip

types of nodes are classified according to the mapping methods and elements used, the nodes that are not on the crack tip location and the collapsed crack tip nodes. The non crack tip nodes can also be separated into the nodes lying on quadratic triangular elements and those on collapsed singular crack tip elements. The mapping scheme can be achieved by the two procedures as follows (Nishioka *et al.* 2001).

4.1 Searching an element in the previous mesh for a new nodal point

If the newly created node p of the new adaptive mesh is not the crack tip node, one can search the triangular-shaped element (6-node triangular or 9-node collapsed element) in the previous mesh that includes the node p by determining the signed area of sum of triangles or by the cross vector product. If node p is the crack tip node, the preceding procedure cannot be used because more than one node is placed at the same crack tip location. Fig. 5(a) shows a new generated mesh superimposed on the previous crack tip elements. If all the collapsed crack tip nodes from both mesh elements are radially placed at a distance r_o from the crack tip, now one can determine the previous mesh crack tip element containing the crack tip node p by measuring the angles with respect to the crack plane as shown in Fig. 5(b). It should be noted that the shaded element in the figure is the desired crack tip element in the previous mesh containing the crack tip node p . Therefore one can easily judge whether the node p is in the element by using the relation $\theta_a \leq \theta_p \leq \theta_b$ where θ_p is the angle formed by the crack plane and a line radially extended from the node p , θ_a and θ_b are the angles of each radial edge of the old mesh crack tip element containing the node p with respect to the crack plane.

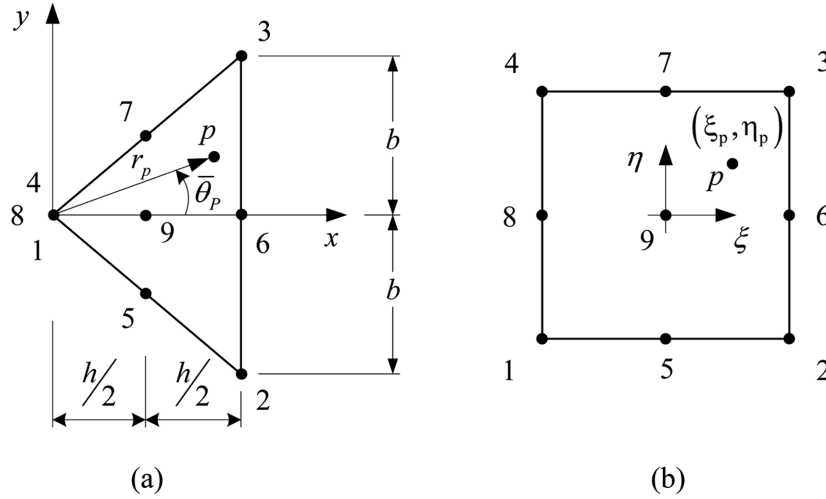


Fig. 6 A new node p in 9-node collapsed crack tip element of (a) physical coordinates and (b) normalized coordinates

4.2 Creating nodal quantities for the new nodal point

For the crack tip element, the normalized coordinates of this element corresponding to the node p must be obtained as shown in Fig. 6. In this figure, the relations between the node p normalized coordinates (ξ_p, η_p) and its cylindrical coordinates with respect to the crack tip element orientation $(r_p, \bar{\theta}_p)$ can be derived from the full shape functions and the Cartesian coordinates of the nodes as

$$\xi_p = \frac{r_p}{\frac{h}{2}\sqrt{q + \tan^2 \bar{\theta}_p}} - 1 \tag{11}$$

$$\eta_p = \frac{h}{b} \tan \bar{\theta}_p$$

where h and b are the height and half base of the crack tip element respectively. In case of the node p is the crack tip node at which $r_p = 0$, the normalized coordinates can be computed from Eq. (11) using the three relative angles defined in Fig. 6(b) as

$$\xi_p = -1$$

$$\eta_p = \frac{\tan\left[\theta_p - \left(\frac{\theta_b + \theta_a}{2}\right)\right]}{\tan\left(\frac{\theta_b - \theta_a}{2}\right)} \tag{12}$$

After obtaining the normalized coordinates or the area coordinates corresponding to the location of the node p on the old mesh element, then the shape functions and nodal displacements of this old mesh element are used to interpolate the displacements of the node p . After all the nodal displacements of the new adaptive mesh has been interpolated from the previous mesh fields, good

initial displacement fields are then provided in the new refined mesh to continue the analysis from the previous mesh model.

5. Algorithm evaluation

Several examples have been used to evaluate the performance of the combined domain integral technique and the adaptive finite element method. These examples are used to determine the J -integral in the opening mode by employing the deformation theory of plasticity and the uniaxial Ramberg-Osgood stress-strain law

$$\frac{\varepsilon}{\varepsilon_o} = \frac{\sigma}{\sigma_o} + \alpha \left(\frac{\sigma}{\sigma_o} \right)^n + \frac{\beta T}{\varepsilon_o} \quad (13)$$

where σ_o is the yield stress, E is the Young's modulus, $\varepsilon_o = \sigma_o/E$ is the yield strain, α is a material constant and n is the strain hardening exponent.

Three square or rectangular integration domains are used to estimate the J -integral by the domain integral technique. The first domain consists of crack tip elements and adjoining elements within the domain. The second domain includes the first domain and adjoining elements between the two domains. The third domain also follows in the same fashion. The "pyramid" q_1 functions with a square and rectangular base corresponding to the integration domains are employed (Shih *et al.* 1986). The functions vary linearly between zero on the edge of the domain and unity at the crack tip. The average of the J -integral computed from the three integration domains is used. The accuracy of the results is evaluated by the extent of the domain dependence defined as a maximum percentage error of the J -integral computed from the three different integration domains compared with their mean value

$$\text{Domain Dependence (\%)} = \text{Max} \left(\frac{|J^{i\text{th}} - J_{\text{avg}}|}{J_{\text{avg}}} \times 100 \right), \quad i = 1, 2, 3 \quad (14)$$

where J_{avg} is the average of the J -integral computed from the three integration domains and $J^{i\text{th}}$ is the J -integral computed from the i th integration domain. These J -integrals are compared with those obtained from other researchers to confirm the agreements.

5.1 Compact Tension specimen - CT

The problem statement of the CT specimen as shown in Fig. 7 is analyzed under the plane strain condition. The specimen characteristic width and crack length per characteristic width ratio are taken to be $W = 51$ mm and $a/W = 0.75$, respectively. The following values of material properties are employed: $E = 202$ GPa, the Poisson's ratio $\nu = 0.3$, $\sigma_o = 414$ MPa, $\alpha = 0.05$ and $n = 10$. Because of symmetry, only half of the specimen is used for modeling. Fig. 8 shows the final adaptive mesh consisting of 1,610 elements with the three integration domains employed in the domain dependence calculations. Fig. 9 shows good agreement of the computed J -integrals as compared to those from the EPRI J estimation scheme (Kumar *et al.* 1981). Good agreements are achieved with the maximum domain dependence of the computed J -integral for the entire load levels of 0.064%.

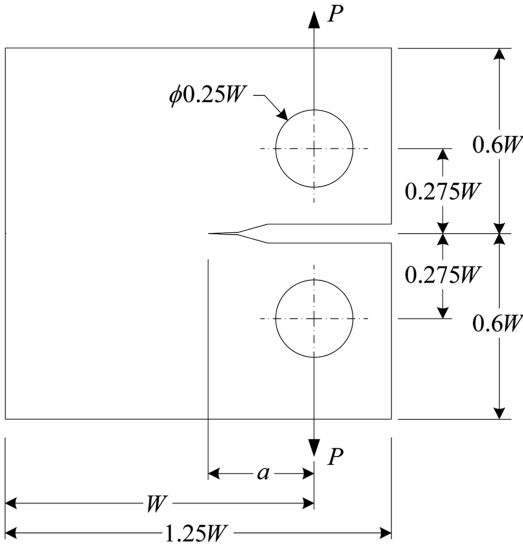


Fig. 7 The compact tension specimen

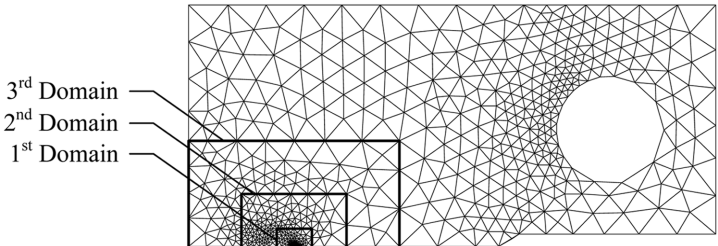


Fig. 8 The final adaptive mesh of the CT specimen with three integration domains

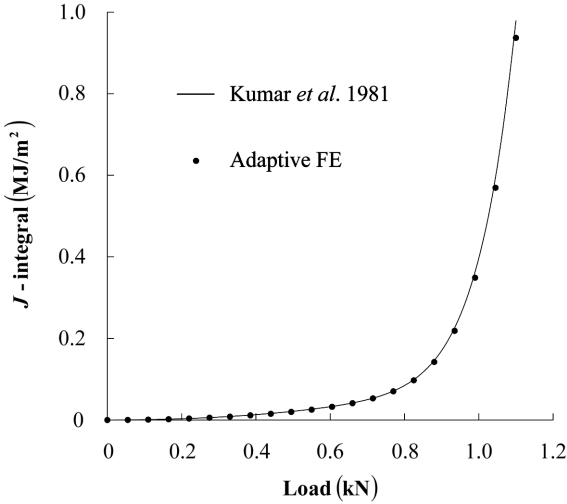


Fig. 9 Comparison of J-integral from adaptive finite element and estimation method for the CT specimen under the plane strain condition

5.2 Double Edge Notched Tension specimen - DENT

Fig. 10 shows the geometry of the DENT specimen analyzed under the plane stress condition with

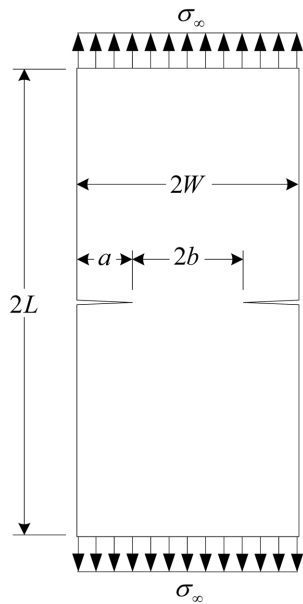


Fig. 10 The double edge notched tension specimen

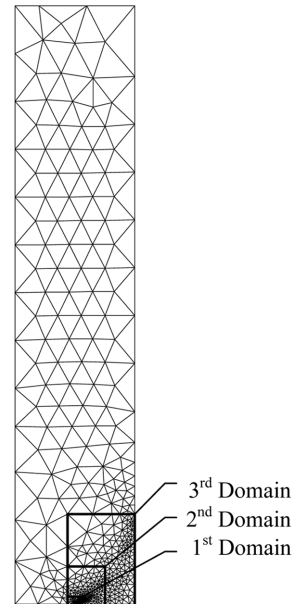


Fig. 11 The final adaptive mesh of the DENT specimen with three integration domains

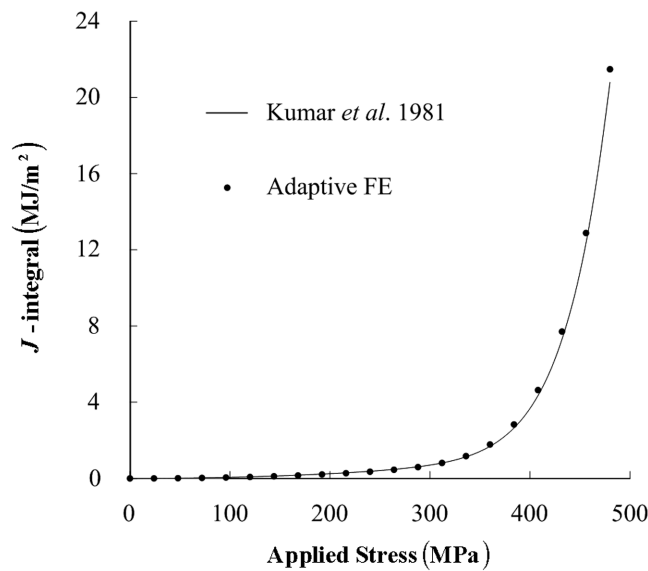


Fig. 12 Comparison of J -integral from adaptive finite element and estimation method for the DENT specimen under the plane stress condition

the same material properties as in the previous example. The half specimen width, crack length per half specimen width and half specimen length per width ratio are $W = 500$ mm, $a/W = 0.5$ and $L/W = 5$, respectively. Fig. 11 shows the final adaptive mesh of the upper right quarter of the specimen consisting of 1,268 elements and the three integration domains used in the domain dependence calculations. Fig. 12 shows good comparison of the computed J -integrals with those from the EPRI J estimation scheme with the maximum domain dependence for the entire load levels of 0.082%.

5.3 Axially cracked cylinder

The plane strain problem statement of an internally pressurized cylinder containing an axial crack is shown in Fig. 13. Here, b denotes the wall thickness, $c = b - a$ the uncracked ligament, p the internal pressure, and R_i and R_o the inner and outer radii, respectively. The geometry dimension for this problem is given by $a/b = 0.25$, $R_i/b = 10$, and b being 2 in. The cylinder wall is subjected to the temperature variation in the form

$$T(r) = 0.25[250 + 800(r - R_i) - 200(r - R_i)^2] \tag{15}$$

where r is the radial distance from the center of the cylinder. The material properties for this problem are given as follows: $E = 30 \times 10^3$ ksi, $\nu = 0.3$, $\sigma_o = 60$ ksi, $\alpha = 0.5$, $n = 5$ and $\beta = 7.3 \times 10^{-6}$ in/in/°F.

The final adaptive mesh of the upper half cylinder consisting of 1,810 elements and its integration domains are presented in Fig. 14. Good comparison between computed J -integrals and those from the thermal-elastic-plastic estimation scheme (Kumar *et al.* 1991) is shown in Fig. 15 with the maximum domain dependence of 0.027%.

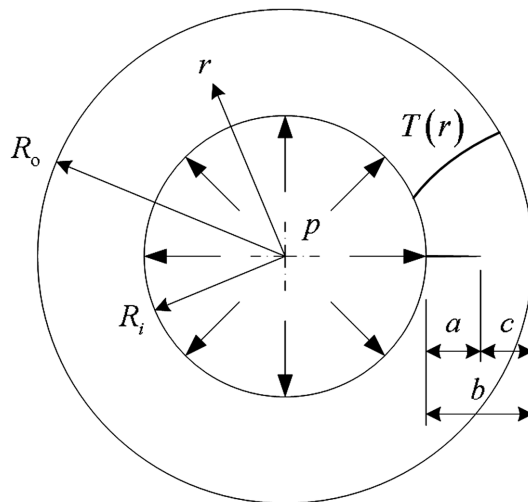


Fig. 13 The axially cracked cylinder with internal pressure and temperature gradient

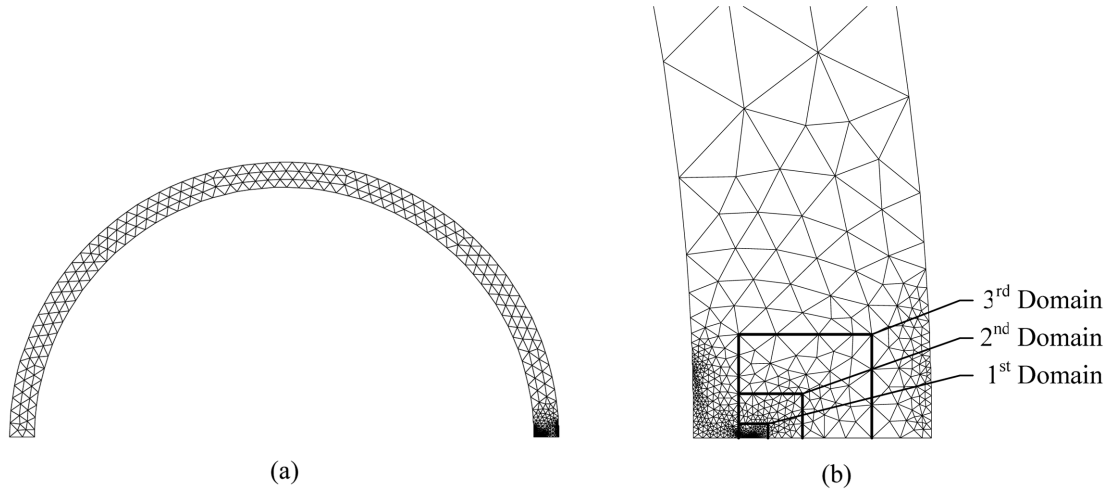


Fig. 14 The final adaptive mesh of the internally pressurized cylinder containing an axial crack depicted in (a) full specimen and (b) crack region with integration domains

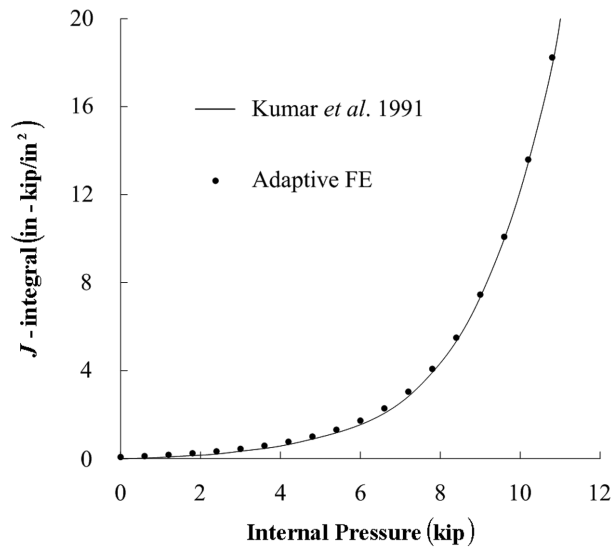


Fig. 15 Comparison of J -integral from adaptive finite element and estimation method for the plane strain axially cracked cylinder under internal pressure and thermal gradient

5.4 Circumferentially cracked cylinder

The last example is a cylinder containing an axisymmetric crack as shown in Fig. 16. The cylinder is loaded by a uniformly applied tensile stress σ^∞ at both ends. The geometry dimensions are given by $R_i/b = 10$, $a/b = 0.25$, $b = 8$ in., and $L/b = 15$. The cylinder wall is subjected to the temperature variation in the form

$$T(r) = [125 + 100(r - R_i) - 6.25(r - R_i)^2] \quad (16)$$

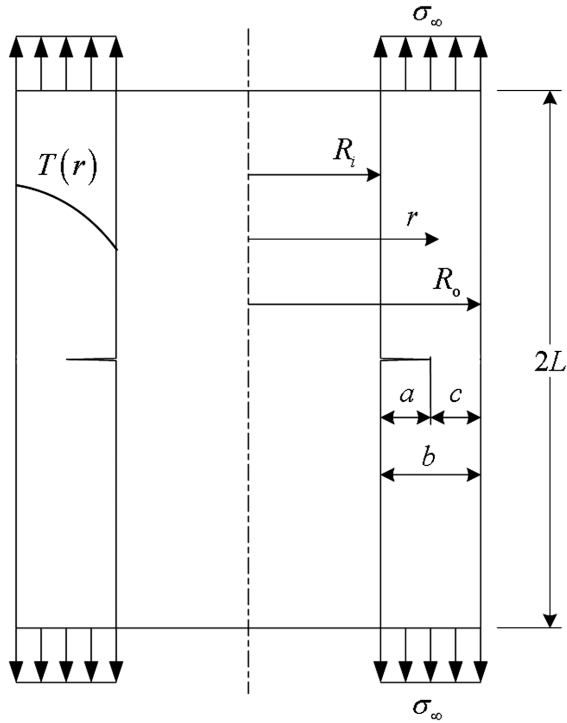


Fig. 16 The circumferentially cracked cylinder

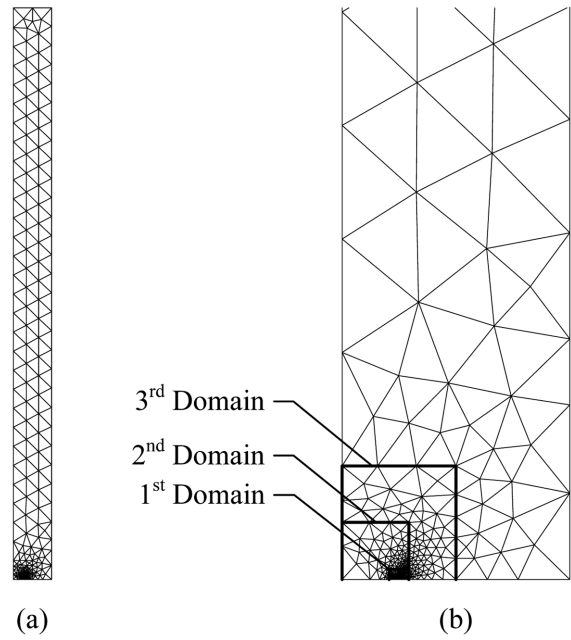


Fig. 17 The adaptive mesh of the circumferentially cracked cylinder depicted in (a) full specimen and (b) crack region with three integration domains

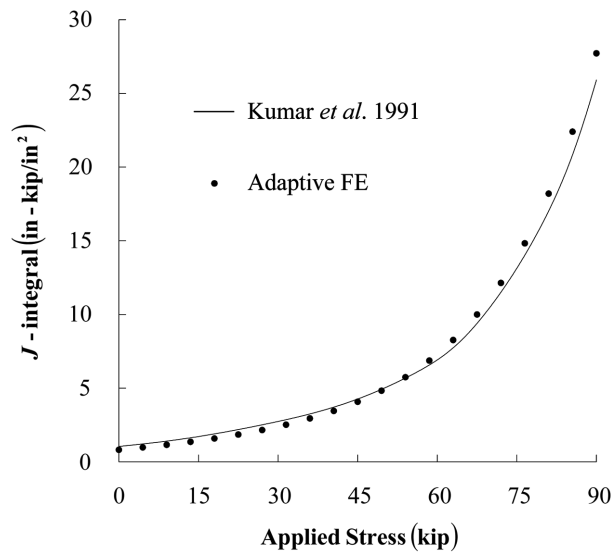


Fig. 18 Comparison of *J*-integral from adaptive finite element and estimation method for the circumferentially cracked cylinder under internal pressure and thermal gradient

where r is the radial distance from the axis of symmetry and R_i is the inner radius of the cylinder. The material properties are identical to those employed in the axially cracked cylinder problem. The final adaptive mesh consisting of 1,426 elements and its three integration domains are shown in Fig. 17. The results are compared with those from the thermal-elastic-plastic estimation scheme as shown in Fig. 18. The figure shows good agreement with the maximum domain dependence of 0.092%.

6. Conclusions

The combined adaptive finite element and domain integral technique with a solution mapping for analyzing non-linear elastic fracture mechanics problems was presented. The concept of the domain integral technique for two-dimensional and axisymmetric geometry was described. The finite element method using the combined 6-node triangular elements and the singular degenerated elements was explained. These singular elements were employed to form up a circular zone surrounding the crack tip to provide high solution accuracy. The solution accuracy was further enhanced by incorporating an adaptive remeshing technique together with a solution mapping scheme. The adaptive remeshing technique places small elements around the crack tips and in the regions with large change of stress gradients for solution accuracy. At the same time, larger elements are generated in the other regions to minimize the total number of unknowns and the computational time. The solution mapping scheme interpolated the displacement solutions computed at a particular load level from a previous mesh onto a new adaptive mesh to provide good initial fields. The efficiency of the combined procedure was evaluated by determining the J -integrals for several benchmark problems. These problems demonstrated the capability of the combined domain integral technique and adaptive finite element method for the analysis of fracture mechanics problems effectively.

Acknowledgements

The authors are grateful to the Thailand Research Fund for supporting this research work. Helpful discussion with Dr. Jirapong Kasivittamnuay is also gratefully acknowledged.

References

- Anderson, T.L. (2005), *Fracture Mechanics: Fundamentals and Applications*, 3rd edition, Taylor & Francis.
- Aoki, S., Kishimoto, K. and Sakata, M. (1981), "Energy-release rate in elastic-plastic fracture problems", *J. Appl. Mech.*, **48**, 825-829.
- Atluri, S.N. (1982), "Path-independent integrals in finite elasticity and inelasticity, with body force, inertia and arbitrary crack-face conditions", *Eng. Fract. Mech.*, **16**, 341-364.
- Borouchaki, H., George, P.L. and Mohammadi, B. (1997), "Delaunay mesh generation governed by metric specifications. Part II. Application", *Finite Elem. Anal. Des.*, **25**, 85-109.
- Dechaumphai, P., Phongthanapanich, S. and Bhandhubanyong, P. (2003), "Adaptive finite elements by Delaunay triangulation for fracture analysis of cracks", *Struct. Eng. Mech.*, **15**, 563-578.
- Frey, W.H. (1991), "Mesh relaxation: A new technique for improving triangulations", *Int. J. Num. Meth. Eng.*,

- 31, 1121-1133.
- Kumar, V., German, M.D. and Shih, C.F. (1981), "An engineering approach for elastic-plastic fracture analysis", *EPRI Report NP-1931*, Electric Power Research Institute, Palo Alto, CA.
- Kumar, V., Schumacher, B.I. and German, M.D. (1991), "Effect of thermal and residual stresses on the J -integral elastic-plastic fracture analysis", *Comp. Struct.*, **40**(2), 487-501.
- Li, F.Z., Shih, C.F. and Needleman, A. (1985), "A comparison of methods for calculating energy release rates", *Eng. Fract. Mech.*, **21**(2), 405-421.
- Moran, B. and Shih, C.F. (1987), "Crack tip and associated domain integrals from momentum and energy balance", *Eng. Fract. Mech.*, **27**(6), 615-642.
- Nishioka, T. (1997), "Computational dynamic fracture mechanics", *Int. J. Fract.*, **86**, 127-159.
- Nishioka, T., Tokudome, H. and Kinoshita, M. (2001), "Dynamic fracture-path prediction in impact fracture phenomena using moving finite element method based on Delaunay automatic mesh generation", *Int. J. Solids Struct.*, **38**, 5273-5301.
- Nishioka, T. and Stan, F. (2003), "A hybrid experimental-numerical study on the mechanism of three-dimensional dynamic fracture", *Comput. Model. Eng. Sci.*, **4**, 119-140.
- Phongthanapanich, S. and Dechaumphai, P. (2004), "Modified multidimensional dissipation scheme on unstructured meshes for high-speed compressible flow analysis", *Int. J. Comput. Fluid D.*, **18**, 631-640.
- Phongthanapanich, S., Traivivatana S., Boonmaruth, P. and Dechaumphai, P. (2006), "Nodeless variable finite element method for heat transfer analysis by means of flux-based formulation and mesh adaptation", *Acta Mech. Sin.*, **22**, 138-147.
- Rice, J.R. (1968), "A path independent integral and the approximate analysis of strain concentration by notches and cracks", *J. Appl. Mech.*, **35**, 379-386.
- Shih, C.F., Moran, B. and Nakamura, T. (1986), "Energy release rate along a three-dimensional crack front in a thermally stressed body", *Int. J. Fract.*, **30**, 79-102.